Lattice Boltzmann implementation of the three-dimensional Ben-Naim potential for water-like fluids

Nasrollah Moradi,[1,a)] Andreas Greiner,[2,b)] Francesco Rao,[1,c)] and Sauro Succi[3,1,d)]
[1]*Freiburg Institute for Advanced Studies (FRIAS), University of Freiburg, Albertstrasse 19, 79104 Freiburg, Germany*
[2]*Department of Microsystems Engineering (IMTEK), University of Freiburg, Georges-Khler-Allee 103, 79110 Freiburg, Germany*
[3]*IAC-CNR, via dei Taurini 9, 00185 Roma, Italy*

(Received 7 December 2012; accepted 25 February 2013; published online 26 March 2013)

We develop a three-dimensional lattice Boltzmann (LB) model accounting for directional interactions between water-like molecules, based on the so-called Ben-Naim (BN) potential [A. Ben-Naim, *Molecular Theory of Water and Aqueous Solutions: Part I: Understanding Water* (World Scientific Publishing Company, 2010); "Statistical mechanics of 'waterlike' particles in two dimensions. I. Physical model and application of the Percus-Yevick equation," J. Chem. Phys. **54**, 3682 (1971)]. The water-like molecules are represented by rigid tetrahedra, with two donors and two acceptors at the corners and interacting with neighboring tetrahedra, sitting on the nodes of a regular lattice. The tetrahedra are free to rotate about their centers under the drive of the torque arising from the interparticle potential. The orientations of the water molecules are evolved in time via an overdamped Langevin dynamics for the torque, which is solved by means of a quaternion technique. The resulting advection-diffusion-reaction equation for the quaternion components is solved by a LB method, acting as a dynamic minimizer for the global energy of the fluid. By adding thermal fluctuations to the torque equation, the model is shown to reproduce some microscopic features of real water, such as an average number of hydrogen bonds per molecules (HBs) between 3 and 4, in a qualitative agreement with microscopic water models. Albeit slower than a standard LB solver for ordinary fluids, the present scheme opens up potentially far-reaching scenarios for multiscale applications based on a coarse-grained representation of the water solvent. © *2013 American Institute of Physics*. [http://dx.doi.org/10.1063/1.4795008]

I. INTRODUCTION

Water is a very special fluid, paramount to most human activities and key to life in our planet. As compared to standard fluids, it exhibits many anomalies, primarily the fact of being denser in the liquid than in the solid phase, exposing a density maximum above the freezing point, a large latent heat and heat capacity, high surface tension, and many others.[1–3] Although a fully comprehensive theory of water thermodynamics is still missing, there is an increasing consensus that many of these anomalies can be traced back to the peculiar nature of the hydrogen bond (HB).[4,5] The HB interaction plays a vital role on structure formation within water. For instance, in water at low temperature, the HBs lead to the formation of an open, approximately four-coordinated (tetrahedral) structure, in which entropy, internal energy, and density decrease with decreasing temperature.[1,6,7] The equilibrium thermodynamics, i.e., phase diagram of water is exceedingly rich, and an *ab initio* comprehensive analysis of its properties is still beyond computational reach. As a result, many models have been developed,[8,9] including lattice ones displaying water-like behavior. Such lattice models are typically based on a many-body lattice-gas Hamiltonian mimicking the essential features of water interactions, with no claim (aim) of (at) atomistic fidelity.[10] To the best of our knowledge, these models have been employed mostly for the study of equilibrium properties, typically via Monte Carlo simulations. Yet, in most phenomena of practical interest, water flows and, most importantly, a variety of molecules, say colloids, ions, and biopolymers, flow along with it, typically in nano-confined geometries. In the biological context, it is well known that the competition between hydrophobic and hydrophilic interactions plays a crucial role in affecting the conformational dynamics of proteins.[11–13] On a larger scale, hydrodynamic interactions are known to exert a significant effect on the collective dynamics and aggregation phenomena within protein suspensions. More generally, hydrodynamic interactions are crucial in the presence of confining walls, due to their strong coupling with resulting inhomogeneities.[14] Based on the above, there is clearly a wide scope for a minimal model of water behavior, capable of including hydrodynamic interactions and geometrical confinement. A methodology to develop an appropriate multiscale approach to water modeling, is offered by the Lattice Boltzmann method, a simulation technique based on a minimal form of Boltzmann kinetic equation living on a discrete space-time lattice.[15–18] Lattice Boltzmann equations (LBEs) have proven fairly successful in simulating a broad variety of complex flows across

a)nasrollah.moradi@frias.uni-freiburg.de
b)andreas.greiner@imtek.uni-freiburg.de
c)ruvido@gmail.com
d)succi@iac.cnr.it

scales, from macroscopic fluid turbulence, all the way down to biopolymer translocation in nanopores.[19–21] The lattice Boltzmann (LB) approach is mostly valued for its flexibility towards the treatment of complex geometries and seamless inclusion of complex physical interactions, e.g., flows with phase transitions, flows with suspended bodies, dynamics of droplets and many others.[22–25] The appeal of the method is considerably enhanced by its conceptual simplicity and computational efficiency, especially on parallel computers.[26,27] Recently a two-dimensional LB model implementing the two-dimensional Ben-Naim model (BN2d)[28] has been presented and applied to the simulation of simple confined water-like fluids.[29] The three-dimensional Ben-Naim model (BN3d) was first published in 1974.[30,31] In this paper, we present the first LB implementation of the BN3d. More specifically, we develop a new LB framework, including HB-like interactions, and explore the properties of such model in free space (bulk water). This serves as a calibration step, preparing for future applications to complex situations involving nano-confinement and hydrodynamic interactions.

The paper is organized as follows. In Sec. II, we present the basic elements of our fluid model, while in Sec. III we discuss the lattice implementation of the BN3d model. Section IV then describes the dynamics of rotational degrees of freedom within a quaternion representation. Section V presents numerical results for various parametrization of the lattice BN3d potential, with special attention to the formation of hydrogen bonds in the course of the evolution. The paper is summarized in Sec. VII.

II. THE FLUID MODEL

Water flow is described by the incompressible Navier-Stokes equations (NSE)

$$\partial_t \mathbf{u} + \mathbf{u}\cdot\nabla\mathbf{u} = \nu\Delta\mathbf{u} - \nabla p, \tag{1}$$

where $\mathbf{u}$ is the fluid velocity, p the fluid pressure, and ν is the kinematic viscosity and density has been set to the conventional value $\rho = 1$, on account of the incompressibility condition $\nabla\cdot\mathbf{u} = 0$.[32]

Instead of discretizing the NSE as a set of non-linear partial differential equations, we find it expedient to solve a minimal lattice version of an underlying kinetic Boltzmann equation.[15] Our fluid model is based on an extension of the lattice Boltzmann method for ideal fluids. We use a three-dimensional lattice with 27 connections (including the cell-center), known as D3Q27 in the LB literature. The elementary cell of the D3Q27 lattice is reported in Fig. 1 and the implications of the lattice connectivity on the tetrahedral structure of the water-like molecules shall be discussed later.

At each grid node $\mathbf{x}$, the velocity distribution function $f_i(\mathbf{x};t)$, i.e., the probability to find a particle at location $\mathbf{x}$, moving along the lattice direction defined by the discrete speed $\mathbf{c}_i$, is evolved according to the lattice Bhatnagar-Gross-Krook model equation:[33,34]

$$f_i(\mathbf{x}+\mathbf{c}_i\Delta t, t+\Delta t) - f_i(\mathbf{x},t) = -\omega\big[f_i(\mathbf{x};t) - f_i^{eq}(\mathbf{x};t)\big], \tag{2}$$

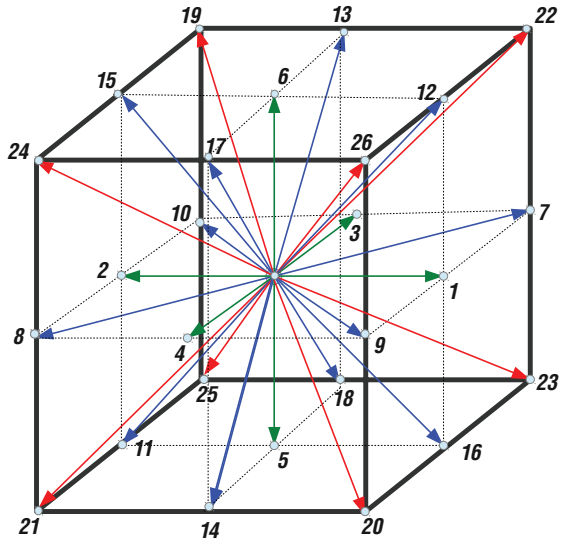

FIG. 1. The unit cell of the D3Q27 lattice. The nearest neighbors, next-nearest neighbors and next-next nearest neighbors are shown in green, blue, and red, respectively. The weighting factors, w_i, for the D3Q27 are: $w_0 = 8/27$ (the cell-center), $w_i = 2/27$ ($i = 1-6$), $w_i = 1/54$ ($i = 7-18$), and $w_i = 1/216$ ($i = 19-26$).

where Δt is the time step, $\omega = \Delta t/\tau_{LB}$ and τ_{LB} is the relaxation time towards local equilibrium. The relaxation time fixes the fluid kinematic viscosity as follows:

$$\nu = c_s^2(\tau_{LB} - \Delta t/2), \tag{3}$$

where c_s is the sound speed of the lattice fluid. By taking $\Delta x = \Delta t = 1$, as it is customary in the LB literature, for the D3Q27 one has $c_s = 1/\sqrt{3}$. The local equilibrium distribution function is a Maxwellian, expanded to the second order in the fluid velocity:

$$f_i^{eq} = \rho w_i\left(1 + \frac{\mathbf{c}_i\cdot\mathbf{u}}{c_s^2} + \frac{(\mathbf{c}_i\mathbf{c}_i - c_s^2 I):\mathbf{uu}}{2c_s^4}\right), \tag{4}$$

where w_i is a lattice-dependent set of weighting factors, normalized to unit value and such that $c_s^2 = \sum_i w_i c_{ia}^2$, $a = x, y, z$. The macroscopic observables, i.e., the fluid density and velocity are defined as follows:

$$\rho(\mathbf{x};t) = \sum_i f_i(\mathbf{x};t), \tag{5}$$

$$\rho(\mathbf{x};t)\mathbf{u}(\mathbf{x};t) = \sum_i \mathbf{c}_i f_i(\mathbf{x};t), \tag{6}$$

where mass has been set to unit value for convenience.

III. THE TETRAHEDRAL WATER-LIKE MODEL

In this section, we describe the details of directional interactions aimed at modeling the effects of hydrogen-bonds. Although conceptually patterned after its two-dimensional predecessor,[29] the three-dimensional extension requires significant technical upgrades, which we now proceed to illustrate.

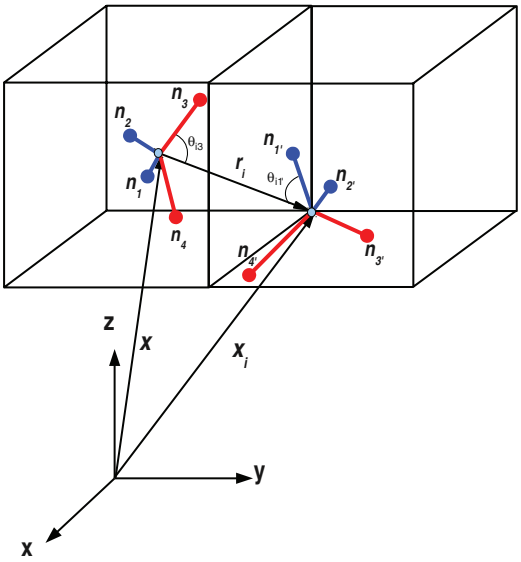

FIG. 2. Tetrahedral representation of water-like molecules sitting at lattice site $\mathbf{x}$ and its neighbor $\mathbf{x}_i$. The four arms are denoted by the corresponding normals n_k, $k = 1, 4$ (unprimed) and n_l, $l = 1, 4$ (primed), respectively. Blue and red code for donor and acceptor arms, respectively. Here the index i corresponds to $i = 23$ in Fig. 1.

A. The interaction potential

We model the interaction of water molecules on a lattice along the specifications given in Refs. 28, 29, 35, and 36, i.e., the hydrogen bond interaction potential for two neighbor water molecules located at $\mathbf{x}$ and its neighbor along lattice direction i, $\mathbf{x}_i$, as shown in Fig. 2. For this purpose, we use the three-dimensional Ben-Naim (BN3d) potential, as presented in Ref. 37:

$$V(\mathbf{x}, \mathbf{x}_i) = \sum_{k=1}^{4}\sum_{l=1}^{4} V_{kl}(\mathbf{x}, \mathbf{x}_i) = -G(\mathbf{r}_i, \rho)\sum_{k=1}^{4}\sum_{l=1}^{4} \epsilon_{kl}^{HB} e^{-\frac{(W_{ik}+W_{il})}{2\sigma_\theta^2}}. \quad (7)$$

Note the minus sign in front of the potential, which connotates the global minimum as the most negative value. In the above, $\mathbf{r}_i = \mathbf{x} - \mathbf{x}_i$ is the distance between the centers of two neighbor tetrahedra, while ϵ_{kl}^{HB} is a selective matrix accounting for the fact that donor (acceptors) arms, corresponding to hydrogens (oxygens) may or may not be allowed to interact with each other. In the present study, all interactions have been enabled, including the repulsive ones, donor-donor and acceptor-acceptor.

As a result, we set

$$\epsilon_{kl}^{HB} = \mp 1 \quad (8)$$

for repulsive (attractive) interactions, respectively. With this convention, repulsive(attractive) interactions contribute positive (negative) energy, respectively.

The radial interaction is chosen in the form[29]

$$G(\mathbf{r}_i; \rho) = W(\rho) e^{-\frac{1}{2}\left(\frac{r_i - R_{HB}}{\sigma_R}\right)^2}, \quad (9)$$

where R_{HB} is the selected length of the hydrogen bond and σ_R controls the sharpness of the radial interaction. Each of the three choices, $R_{HB} = 1, \sqrt{2}, \sqrt{3}$, places a preferential bias on the formation of hydrogen bonds between face-centers (N2 = nearest-neighbors), edge-centers (N3 = next-nearest neighbors) or corners (N4 = next-next nearest neighbors) of the D3Q27 lattice, respectively. Note that each set of neighbors counts more than 4 sites, hence it can, in principle, saturate the four hydrogen bonds per molecule, with no extra contribution from other neighbors.

In Eq. (7), the density $\rho(\mathbf{r})$ at lattice site $\mathbf{r}$ enters the weighting function through the empirical factor:

$$W(\rho) \propto \left(1 + e^{-\alpha\left(\frac{\rho_{max} - \rho}{\rho_{max} - \rho_{min}}\right)}\right)^{-1}, \quad (10)$$

which takes into account the density-dependent propensity of water to form ordered states[29] at a lower density ρ_{min}, while the disordered states have a higher density ρ_{max}. The parameter $\alpha > 0$ controls the range of this density variation near solid walls. Since in this paper we shall deal with bulk fluid only, here and throughout we set $\alpha = 0$, i.e. $W(\rho) = 1$. In Fig. 3 the function $G(\mathbf{r}_i; \rho)$ has been plotted for $R_{HB} = (\sqrt{2} + \sqrt{3})/2$ and $\sigma_R = 0.28$ with $W(\rho) = 1$.

The terms governing the directional interactions read as follows:

$$V_{ikl} = e^{-\frac{W_{ik}+W_{il}}{2\sigma_\theta^2}}, \quad (11)$$

where we have defined

$$W_{ik} = (\hat{\mathbf{n}}_k \cdot \hat{\mathbf{r}}_i - 1)^2 \quad (12)$$

and

$$W_{il} = (\hat{\mathbf{n}}_l \cdot \hat{\mathbf{r}}_i + 1)^2. \quad (13)$$

These are the central objects governing directional interactions.

The unit vector for the direction of the tetrahedral arm k, is denoted by $\hat{\mathbf{n}}_k = \mathbf{r}_k/r_k$, while we have defined $\hat{\mathbf{r}}_i = \mathbf{r}_i/r_i$ as the unit vector along the ith link of the lattice. In the above, σ_θ is a parameter controlling the stiffness of directional interactions (small sigmas code for "stiff clicks"). It can be seen from Fig. 2 that $\mathbf{n}_k \cdot \hat{\mathbf{r}}_i = \cos(\theta_{ik})$, where θ_{ik} is the angle between the kth arm and the direction of the neighboring

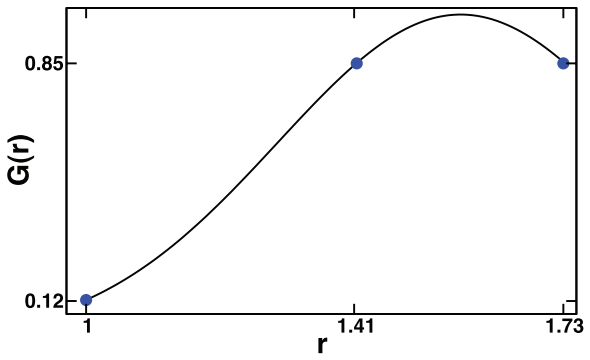

FIG. 3. Radial shape functions for the case $\sigma_R = 0.28$ and $R_{HB} = (\sqrt{2} + \sqrt{3})/2$. Note that nearest-neighbor interactions are roughly an order of magnitude weaker than next and next-next nearest neighbor ones.

TABLE I. Extremal values of the angular potential $V_{ikl} \equiv e^{-(W_{ik}+W_{il})/2\sigma_\theta^2}$, corresponding to $\cos\theta_{ik} = 1, 0, -1$ and $\cos\theta_{il} = -1, 0, 1$ for the case $\sigma_\theta = 1$.

	$\cos\theta_{il}$		
$\cos\theta_{ik}$	−1	0	1
1	1.000	0.607	0.135
0	0.607	0.368	0.082
−1	0.135	0.082	0.018

tetrahedron. The extremal values of V_{ikl} for $\sigma_\theta = 1$ are reported in Table I. Since $W_{ik} + W_{il}$ takes values in the range [0, 8], the corresponding range of variation of V_{ikl} is $[e^{-4/\sigma_\theta^2}, 1]$ for attractive interactions and $[-1, -e^{-4/\sigma_\theta^2}]$ for repulsive ones (please note that the overall contribution is negative for attractive and positive for repulsive, on account of the minus sign upfronting the overall energy). This range exhibits a non-analytic dependence on the value of σ_θ. The angular potential V_{ikl} is reported in Fig. 4 for the case $\sigma_\theta = 0.28$. It can be noted that such case corresponds to a sharp (selective) landscape, taking the system towards the local minimum at $cos\,\theta_{ik} = 1$ and $cos\,\theta_{il} = -1$, respectively. Thus, to enforce sharp HB formation, σ_θ is selected to be sufficiently smaller than 1.

B. Estimating the minimum energy

Before analysing the numerical results, it proves instructive to develop an estimate of the global minimum (most negative) energy, E_{min}, of the model in the absence of thermal fluctuations. Referring to Eq. (7), the pair-potential energy of a tetrahedron with any of its neighbors, consists of 4^2 (donor-acceptor, donor-donor and acceptor-acceptor) interaction terms. Summation upon all neighbors, to compute the potential experienced by a single tetrahedron in the D3Q27 lattice, entails $4^2 \times 27 = 432$ terms. To proceed further, we neglect the repulsive interactions in Eq. (7), which are heavily suppressed, particularly for small values of σ_θ, on account of their positive energy. Based on the Eq. (11), the minimum (most negative) energy of a HB, U_{HB}, is associated with $V_{ikl} = 1$, which results in $E_{HB} = -G(\mathbf{r}_i; \rho)$. We assume that the global minimum is associated with HBs = 4, where all the four hydrogen bonds are perfect, i.e., zero angle or sharp click, between the donor and acceptor

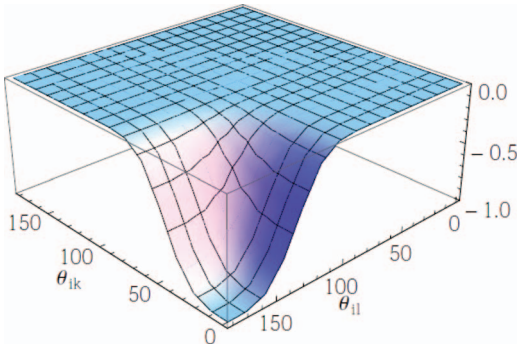

FIG. 4. The angular potential V_{ikl} for $\sigma_\theta = 0.28$. θ_{ik} and θ_{il} are shown in degrees.

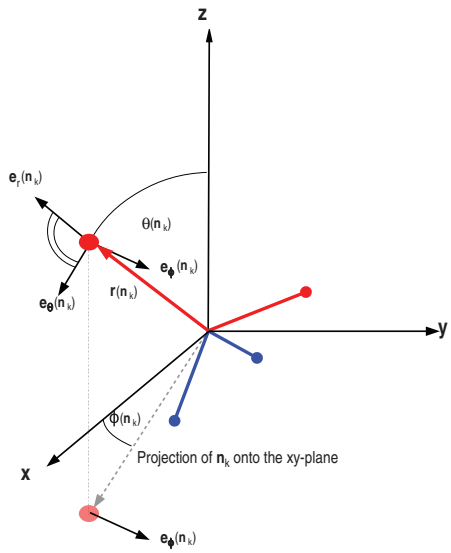

FIG. 5. The torque acting on the arm $\mathbf{n}_k$ has two components in the direction of $\mathbf{e}_\phi(\mathbf{n}_k)$ and $\mathbf{e}_\theta(\mathbf{n}_k)$. The total torque acting on the tetrahedron is then the vector sum of the torques acting on all 4 arms.

arms. As a global geometrical constraint, the tetrahedra on the D3Q27 lattice can achieve HBs = 4 (perfect HB), whenever the arms point to the next-next nearest neighbors (corners), e.g., to the crystallographic directions (1, 1, 1), (−1, −1, 1), (1, −1, −1) and (1, 1, −1). This requires all arms to make an angle $\arccos(\sqrt{1}/\sqrt{3}) \simeq 55^\circ$ with the x, y, and z axis, respectively, where the nearest neighbors are located. Therefore, the strongest donor-acceptor interaction with the nearest neighbors is associated with $\theta_{ik} \simeq 55^\circ$ and $\theta_{il} \simeq 125^\circ$. With the choice of $R_{HB} = (\sqrt{2} + \sqrt{3})/2$, the strength of nearest donor-acceptor interaction is about one tenth of the other interactions (see Figure 5), so that their contribution can safely be neglected.

In contrast, the arms make an angle of $\arccos(\sqrt{2}/\sqrt{3}) \simeq 35^\circ$ with xy, xz, and yz planes, which contain all the 12 next-nearest-neighbors. We then take into account only the leading term in Eq. (7), i.e., the strongest donor-acceptor interaction for each neighbor. We also assume that the strongest donor-acceptor for the next-nearest-neighbors is associated with $\theta_{ik} \simeq 35^\circ$ and $\theta_{il} \simeq 145^\circ$, yielding a comparable value with −1.0 (see Eqs. (12) and (13)). For the next-next-nearest neighbors, the 4 corners make 4 perfect HBs (with minimum energy), while the other four corners interact much more weakly and can therefore be neglected.

Putting all together, we can estimate the global minimum energy as

$$E_{min} \approx -[4G(\sqrt{3}; \rho) + 12G(\sqrt{2}; \rho)V_{ikl}(\sigma_\theta, 35^\circ, 145^\circ)]N. \tag{14}$$

Given the value $\sigma_\theta = 0.28$ used in this work, we compute $V_{ikl}(\sigma_\theta, 35^\circ, 145^\circ) \approx 0.65$. For $R_{HB} = 0.5(\sqrt{2} + \sqrt{3})$, as used in the present study, the minimum energy per molecule is estimated as

$$\frac{E_{min}}{N} \sim -10, \tag{15}$$

which is in good agreement with the numerical results (see Figs. 6 and 8).

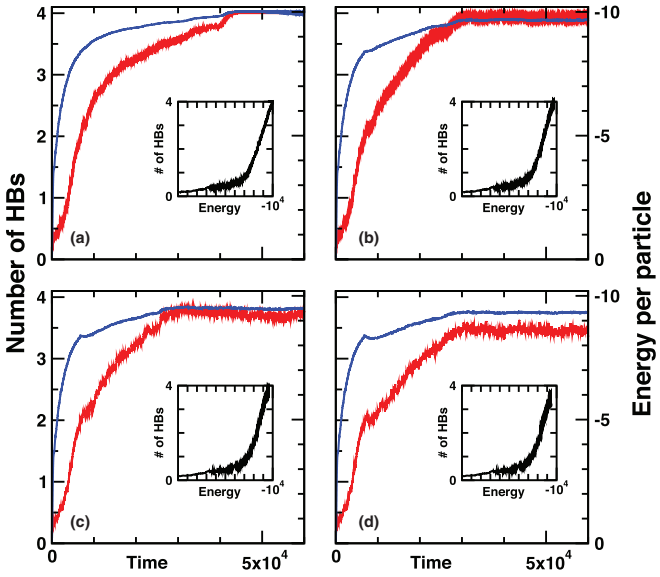

FIG. 6. Time evolution of the total potential energy vs the LB time steps together with the number of hydrogen bonds for four different effective temperatures, at (a) $\beta^{-1} = 10^{-4}$, (b) $\beta^{-1} = 4 \times 10^{-4}$, (c) $\beta^{-1} = 5.5 \times 10^{-4}$, and (d) $\beta^{-1} = 7 \times 10^{-4}$. Main parameters are as follows $N = 10^3$, $\sigma_R = 0.28$, $\sigma_\theta = 0.28$, and $R_{HB} = (\sqrt{3} + \sqrt{2})/2$.

IV. EQUATION OF MOTION OF THE ROTATIONAL DEGREES OF FREEDOM

Next we discuss the dynamics of the rotational degrees of freedom, namely the local order parameters of our model. At each lattice site, the tetrahedra perform rigid-body rotations under the drive of the torque associated with directional interactions with neighboring sites.

To compute such an effect, let us recall that the total potential energy of the tetrahedron sitting at lattice site $\mathbf{x}$, is given by the sum of the pair potentials over the set of lattice neighbors, Eq. (7), namely

$$V(\mathbf{x}) = \sum_i V(\mathbf{x}, \mathbf{x}_i). \tag{16}$$

The torque $\boldsymbol{\tau}$ acting on the angular momentum $\boldsymbol{\ell}$ of the tetrahedron placed at $\mathbf{x}$, is given by

$$\boldsymbol{\tau} = \sum_{i=1}^{26} \boldsymbol{\tau}_i = \sum_{i=1}^{26} \sum_{k=1}^{4} \mathbf{r}(\mathbf{n}_k) \times \mathbf{F}_{ik}, \tag{17}$$

where $\mathbf{r}(\mathbf{n}_k)$ represents the position of the donor (or the acceptor) sitting at the tip of arm k and the force $\mathbf{F}_{ik}$ is given by the negative gradient of the potential energy of the arm k, due to the interaction with its ith neighbor, $-\nabla \sum_{l=1}^{4} V_{ikl}$ (see Eq. (7)). Since there is no radial dependence, it is convenient to calculate the force and the torque in spherical coordinates and then map the components back to the corresponding Cartesian coordinates (see Fig. 5).

We consider a driven-damped motion of the tetrahedron, according to the following Langevin equation:

$$\dot{\boldsymbol{\ell}} = -\gamma \boldsymbol{\ell} + \boldsymbol{\tau} + \boldsymbol{\tau}_r, \tag{18}$$

where $\boldsymbol{\tau}_r$ is a random component, encoding rotational diffusion effects. By construction, it obeys the fluctuation-dissipation relation:

$$\langle \boldsymbol{\tau}_r(t) \boldsymbol{\tau}_r(t') \rangle = 3\gamma\beta^{-1}\mathbf{I}\delta(t - t') \tag{19}$$

β being the effective temperature of the fluid ($\beta^{-1} \equiv K_B T$), $\mathbf{I}$ the moment of inertia, a unit matrix of magnitude I, and δ is the delta function.

Next, we make the usual enslaving assumption, $|\dot{\boldsymbol{\ell}}| \ll \gamma |\boldsymbol{\ell}|$, so that we may neglect the time rate of change of the angular momentum, to obtain

$$\boldsymbol{\omega} = \frac{1}{\gamma I}(\boldsymbol{\tau} + \boldsymbol{\tau}_r), \tag{20}$$

where we have used the convention $\boldsymbol{\ell} = I\boldsymbol{\omega}$, so that $\boldsymbol{\ell} = I\dot{\boldsymbol{\phi}}$. Thus, by discretizing Eq. (20), we have

$$\Delta\boldsymbol{\phi} = \frac{\boldsymbol{\tau} + \boldsymbol{\tau}_r}{\gamma I}\Delta t. \tag{21}$$

This provides a rotation axis and a magnitude for the rotation around it, modulo 2π. The orientation of the tetrahedron is described by a quaternion with components q_μ,[38] $\mu = 0, 1, 2, 3$. Details on the rotational dynamics of the tetrahedron, as per Eq. (21), is given in the Appendix.

A. The kinetic equation for the quaternion moments

The quaternion macrofields $q_\mu(\mathbf{x}; t)$ introduced in the above obey the following advection-diffusion-reaction (ADR) equations:

$$\partial_t q_\mu(\mathbf{x}, t) + \mathbf{u} \cdot \nabla q_\mu(\mathbf{x}; t) = D\Delta q_\mu + \dot{q}_\mu(\mathbf{x}; t), \tag{22}$$

where $\mathbf{u}$ is the fluid velocity and D is the kinematic translational diffusivity of the quaternion components. The last term at the right hand side is the rate of change of the quaternion fields, due to the rigid-body rotation driven by the torque, as given in Eq. (A6).

The above equation is also solved by a Lattice Boltzmann technique, leading to the following set of kinetic equations:

$$q_{i\mu}(\mathbf{x} + \mathbf{c}_i\Delta t, t + \Delta t) = q_{i\mu}(\mathbf{x}, t)\left(1 - \frac{\Delta t}{\tau_D}\right) + q^{eq}_{i\mu}(\mathbf{x}, t)\frac{\Delta t}{\tau_D} + w_i \dot{q}_\mu(\mathbf{x}; t)\Delta t, \tag{23}$$

where w_i are the lattice weights and $\mathbf{c}_i$ the lattice velocities introduced in Sec. II. In the above, τ_D is the quaternion relaxation time, controlling the kinematic diffusivity of quaternion according to

$$D = c_s^2(\tau_D - 1/2) \tag{24}$$

in lattice units $\Delta t = \Delta x = 1$.

Each component of the quaternion field, $q_\mu(\mathbf{x}, t)$, is treated as the scalar density of a corresponding set of discrete distribution functions, according to

$$q_\mu(\mathbf{x}, t) = \sum_i q_{i\mu}(\mathbf{x}, t). \tag{25}$$

In other words, each single component is treated as a fictitious density (note that this fictitious densities do not need to be

positive definite). The local quaternion equilibrium in Eq. (23) is given by

$$q_{i\mu}^{eq} = w_i q_\mu \left(1 + \frac{\mathbf{u}\cdot\mathbf{c}_i}{c_s^2}\right) \tag{26}$$

in which the local velocity $\mathbf{u}$ is again provided by the coupled LB dynamics of the fluid. The quaternion components are updated concurrently with the LB fluid solver, and once this step is completed, the arms of the tetrahedron are updated via the Eq. (A4) (see the Appendix). This way, the quaternion dynamics is coupled self-consistently to the hydrodynamic motion of the water-like fluid. We should mention that an imposed flow $\mathbf{u}$, supplied by a standard LB scheme for fluid flow separately (introduced in Sec. II), does affect the quaternion dynamics (rotation of water molecules) via Eq. (26) but the fluid flow itself is independent of the quaternion dynamics. In the current work we focus on the bulk water (no hydrodynamics) and set $\mathbf{u} = 0.0$.

V. NUMERICAL RESULTS

Any water-like model must necessarily pass a series of validation tests, depending on the application it is intended to. As a calibration of the present three-dimensional model, here we focus on its propensity to form hydrogen bonds under an optimal choice of simulation parameters.

Technically, we stipulate that a hydrogen bond is formed whenever a donor and acceptor arms come head-on together, within a tolerance cone of aperture 20°. The total energy of system is also monitored, in order the appraise the tendency of the system towards minimum energy configurations.

A. Simulation setup

All simulations are performed on a D3Q27 lattice, with periodic boundary conditions. Initial conditions shall be discussed shortly. As noted earlier on, the D3Q27 lattice consists of three classes ("shells") of sites: 6 face-centers at distance $r = 1$, 12 edge-centers at a distance $r = \sqrt{2}$, and 8 corners at a distance $r = \sqrt{3}$. Unless stated otherwise, the simulations are performed with the following set of input parameters: $\sigma_R = 0.28$, $\sigma_\theta = 0.28$, $\tau_D = 10^3$, $\gamma = 10^5$, $\tau_{LB} = 1$, and $R_{HB} = (\sqrt{2} + \sqrt{3})/2$. The lattice consists of $N_x = N_y = N_z = 10$ grid points, for a total of 10^3 lattice sites, each hosting a tetrahedral water-like molecule. Different values of the effective temperature are explored, approximately in the range between $10^{-4} \le \beta^{-1} \le 10^{-3}$. All values are given in dimensionless LB units ($\Delta x = \Delta t = 1$). More precisely, initial conditions are taken random in the angular momentum, and then evolved at a low effective temperature ($\beta^{-1} = 10^{-4}$), until the system attains the condition HBs = 2. This transient thermalization helps minimizing trapping in local minima of the water potential associated with random initial conditions, which carry a low number HBs ≈ 0.2, very far from the global minimum at HBs = 4.

After such transient thermalization, the fluid configuration is further evolved at different values of the effective temperature, until a statistical steady-state is attained.

B. From lattice to physical space-time units

To fix the length units, we stipulate a mesh-spacing $\Delta x = \sigma$, i.e., the range of interaction, which is pretty close to the average molecular distance, hence of the order of 0.3 nm. This choice corresponds to one water molecule per water-like molecule, and it is consequential to the tetrahedral structure of the LB water-like molecule. Indeed, at larger spatial scales, there is no compelling reason to assume that groups of water molecules would or should display a tetrahedral structure on average.

It is worth recalling that the idea of taking LB down to molecular length scales has been applied before, to perform head-on comparisons between LB and molecular dynamics (MD) for the case of flows past nanosized obstacles.[39] Such studies highlighted that quantitative agreement between the two methods requires sub-molecular mesh-spacing, i.e., $\Delta x \le \sigma$.

The conversion to time units, however, is no longer one-to-one. The LB time step is given by $\Delta t_{LB} = \Delta x/c$, i.e. about 0.15 ps, by taking $c = c_s\sqrt{3} \sim 2 \times 10^3$ m/s. This is about two orders of magnitude above the MD time step $\Delta t_{MD} \sim 0.01\tau_{MD}$ where $\tau_{MD} = \sigma/v_{th}$ is of the same order as Δt_{LB}. We shall comment on the computational implications of this important point shortly.

Finally, the energy units are chosen by setting the HB energy, about 10 KJ/mole, to the unit value in the lattice, $|\epsilon_{kl}^{HB}| = 1$, as per Eq. (8).

C. Dynamics of hydrogen bond formation

In Fig. 6, we show the time evolution of the water potential, Eq. (10), with $R_{HB} = (\sqrt{3} + \sqrt{2})/2$, for the four effective temperatures: $\beta^{-1} = 10^{-4}$, $\beta^{-1} = 4 \times 10^{-4}$, $\beta^{-1} = 5.5 \times 10^{-4}$, and $\beta^{-1} = 7 \times 10^{-4}$.

It should be noted that our results show sensitivity to the shape of radial interactions and sharing between competing shells of lattice molecules, so that a certain degree of fine-tuning is required. The choice $R_{HB} = (\sqrt{2} + \sqrt{3})/2$, is found to provide satisfactory results, with HBs pretty close to the top value, HBs = 4. Besides, the amplitude of thermal fluctuations depends on the choice of parameters in the BN3d potential particularly ϵ_{kl}^{HB}. High thermal fluctuations may corrupt the norm of quaternions, which must remain constant during the simulations, thus leading to numerical instabilities.

From Fig. 6, it is apparent that a very substantial number of hydrogen bonds, nearing the top value HBs = 4, is formed at all effective temperatures, with a slight decrease at decreasing the effective temperature.[5] Also apparent is the strong correlation between the energy decrease (more negative) in time and the increasing number of hydrogen bonds, all along the simulation. This provides a neat indication that the number of hydrogen bonds serves indeed as a representative order parameter for the evolution of the system, from a high-energy disordered configuration to a quasi-ordered minimum-energy configuration.

D. Visual information

To obtain a visual appreciation of the spatial ordering of the rotational degrees of freedom, the angular momenta, in

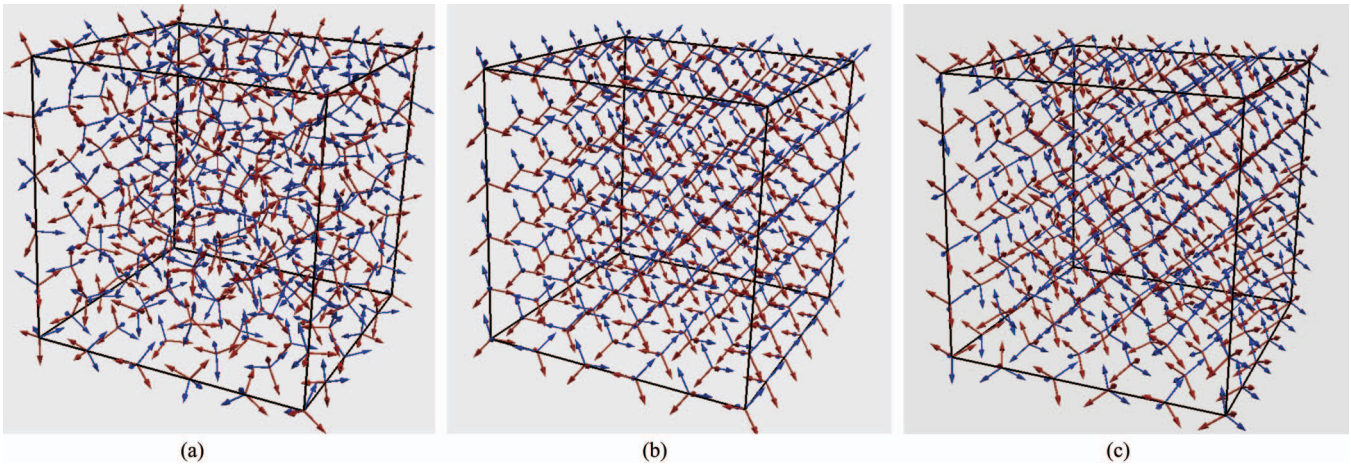

FIG. 7. (a) Initial random distribution of tetrahedrons and the corresponding final distribution at steady state with and without thermal fluctuations in (b) and (c), respectively.

Fig. 7, we report the initial and the final configurations (steady state) of the water-like fluid at $\beta^{-1} = 10^{-4}$ and without thermal fluctuations. In case of no thermal fluctuations (Fig. 7(b)), the final state is a highly ordered, ice-like crystal (HBs = 4). When thermal fluctuations are introduced (Fig. 7(c)), the final configuration deviates from the crystal state (but still almost ordered) associated to a local minimum with a *HBs* < 4, namely HBs $\simeq 3.7$. Clearly, the smaller β, the more pronounced is the deviation from an ordered crystal. Here, for the sake of a better visualization, the simulation has been performed for a small system of size $N = 6^3$. The other LB parameters are the same as in the case of $N = 10^3$.

VI. LATTICE BOLTZMANN AS AN ACCELERATED MOLECULAR DYNAMICS MINIMIZER

The present Lattice Boltzmann Advection-Diffusion-Reaction (LB-ADR) model attains the minimum energy by evolving the system along a mesoscopic trajectory. In this respect, it presents potential advantages with respect to both Monte Carlo (MC) and MD.

As compared to MC, the fact of evolving in large-steps along a physical trajectory, appears to reduce significantly trapping into local minima. To date, this is just a factual observation, for which a comprehensive theoretical explanation remains to be developed. Although a detailed comparison is left for future work, preliminary data indicate that the present LB-ADR dynamics attains the potential minimum much faster than annealed Metropolis Monte Carlo. More importantly, this edge appears to be a fast-growing function of the size of the system. However, as a cautionary note, it should be mentioned that, depending on the choice of the initial conditions, eventually the LB-ADR scheme also gets trapped in local minima. Here, we examine the energy minimization of a small system of size $N = 6^3$, via both LB with no thermal fluctuation, and simulated annealing MC.

In Fig. 8 the two methods are compared. As it can be seen from the figure, both methods finally attain the same (global) minimum potential, thereby providing further confidence in LB-ADR as a realistic dynamic energy minimizer. The present LB-ADR finds the minimum potential on a 6^3 lattice in about 1.5×10^4 LB steps, taking about 3 min CPU time on a standard PC, while plain Metropolis MC minimizes the potential in 3×10^6 MC steps, taking about 60 hours.

As compared to MD, the main advantage is that the dynamics proceeds in much larger steps, so that substantial speed-up factors are also expected.

Indeed, we have noted before that the LB time step is about 0.15 ps, hence two-three orders above the typical MD time step. This exposes a major bonus of the lattice-bound dynamics inherent to the LB scheme, as opposed to the lattice-free MD trajectories. The fact that the LB populations hop synchronously from site-to-site, an *exact, round-off free* operation on digital computers, implies that the scheme remains stable in the full range $\Delta t_{LB} < 2\tau_{LB}$ (the reader may notice that this range guarantees a positive-definite viscosity $\nu = c_s^2(\tau - \Delta t/2)$. This sends an interesting message for

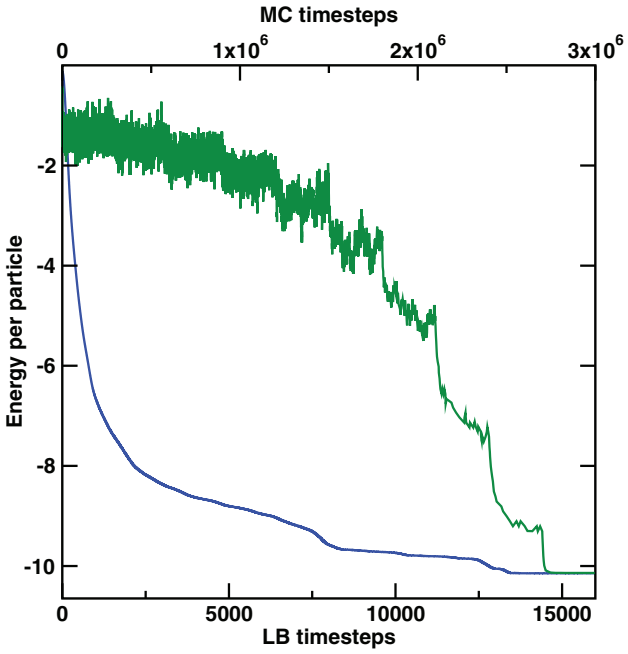

FIG. 8. Comparison of LB-ADR (blue) and MC (green) simulated annealing as energy minimizers. Main parameters are as follows $N = 6^3$, $R_{HB} = (\sqrt{3} + \sqrt{2})/2$, $\sigma_R = 0.28$, $\sigma_\theta = 0.28$.

prospective multiscale applications: even on the conservative assumption that the cost of updating a single degree of freedom (the water-like LB molecule) is the same for LB and MD, the former would still offer about three orders of magnitude savings in the time-span of the simulation. To place this within a concrete perspective, the present LB model evolves 10^3 water-like molecules over a 1.5 ns trajectory in about 15 min CPU time, on a standard PC.

VII. CONCLUSIONS AND OUTLOOK

Summarizing, we have presented a Lattice Boltzmann implementation of the three-dimensional Bein-Naim (BN3d) water potential.

The main results of the present study are as follows:

i) The three-dimensional LB-ADR model can achieve a number of hydrogen bonds in the expected range, i.e. between 3 and 4. It shows a sensitivity to the shape of radial interactions and sharing between competing shells of lattice molecules, so that a certain degree of fine-tuning is required. The choice $R_{HB} = (\sqrt{2} + \sqrt{3})/2$, is found to provide satisfactory results, with HBs pretty close to the top value, HBs = 4, and a qualitatively correct dependence on the effective fluid temperature, albeit in a limited range.

ii) For deep quenches, starts from "hot," random, initial conditions, down to high β, many trajectories do not conform to the rule "lower temperature = more hydrogen bonds," as a result of trapping in local minima. Initial thermalization, as applied in this work, proves very beneficial in developing a sensible temperature dependence of the number of HBs. However, the influence of initial conditions remains to be analyzed in depth.

iii) As an interesting sideline, the present LB-ADR scheme seems to act as a very effective a dynamic minimizer for the water-like lattice potential at hand. Under all conditions explored so far, many more than those reported in the present paper, it was able to find the near-global minimum starting from very far initial conditions, and typically dramatically faster than annealed Monte Carlo. Given the broad use of lattice potentials in statistical mechanics, this might open up an interesting direction for future research on multiscale simulations of micro and nano-biological phenomena.

ACKNOWLEDGMENTS

N.M. and F.R. were supported by the Excellence Initiative of the German Federal and State Governments (DFG). N.M. acknowledges the funding from IMTEK. A.G. gratefully acknowledges funding from the Volkswagen Foundation. S.S. acknowledges financial support via the External Senior Fellow program at FRIAS. Valuable discussions with S. Melchionna are kindly acknowledged.

APPENDIX: REPRESENTATION OF ROTATIONS USING QUATERNIONS

1. Quaternion algebra

A quaternion is an object represented as a collection of 4 real parameters $q = (q_0, q_1, q_2, q_3) = (q_0, \mathbf{q})$, where $\mathbf{q}$ is a 3D vector. The sum of two quaternions q and p is given as

$$\begin{aligned} q + p &= (q_0 + p_0, q_1 + p_1, q_2 + p_2, q_3 + p_3) \\ &= (q_0 + p_0, \mathbf{q} + \mathbf{p}). \end{aligned}$$

The summation is commutative while the product

$$q \circ p = (q_0 P_0 - \mathbf{q} \cdot \mathbf{p}, q_0 \mathbf{p} + p_0 \mathbf{q} + \mathbf{q} \times \mathbf{p})$$

is not. The conjugate of the quaternion q is defined as

$$q^* = (q_0, -q_1, -q_2, -q_3) = (q_0, -\mathbf{q}),$$

while its norm is given as

$$|q| = \sqrt{q_0^2 + q_1^2 + q_2^2 + q_3^2}. \tag{A1}$$

2. Rotations represented as unit quaternions

A pure rotation is usually described by Euler equations of motion. However, there is another way of describing rotation by means of quaternions. Quaternions are often convenient for numerical applications. Consider a rotation of a solid object about a unit vector $\mathbf{u} = (u_x, u_y, u_z)$ by an angle $\phi = 2\alpha$. The corresponding unit quaternion representing this rotation is given by

$$q = \{q_0, q_1, q_2, q_3\} = \begin{cases} q_0 = \cos(\alpha) \\ q_1 = \sin(\alpha) u_x \\ q_2 = \sin(\alpha) u_y \\ q_3 = \sin(\alpha) u_z \end{cases}. \tag{A2}$$

From these equations, we see that its norm is unit, due to Eq. (A1).

Any point $\mathbf{r} = (x, y, z)$ of a solid may be represented as a quaternion p with vanishing real part

$$p = (0, x, y, z) = (0, \mathbf{r})$$

a so called purely imaginary quaternion. After rotation about $\mathbf{u}$ by the angle ϕ the point $\mathbf{r}$ it is transformed to an imaginary quaternion p' according to

$$p' = q \circ p \circ q^* = \left(0, \left(q_0^2 - \mathbf{q} \cdot \mathbf{q}\right)\mathbf{r} + 2q_0(\mathbf{q} \times \mathbf{r}) + 2(\mathbf{q} \cdot \mathbf{r})\mathbf{q}\right), \tag{A3}$$

where the imaginary part of q' represents the transformed position $\mathbf{r}'$, to read

$$\mathbf{r}' = \left(q_0^2 - \mathbf{q} \cdot \mathbf{q}\right)\mathbf{r} + 2q_0(\mathbf{q} \times \mathbf{r}) + 2(\mathbf{q} \cdot \mathbf{r})\mathbf{q} \tag{A4}$$

or in a matrix form $\mathbf{r}' = \mathbf{A} \cdot \mathbf{r}$ where the matrix $\mathbf{A}$ is given by

$$\mathbf{A} = 2\begin{bmatrix} \left(q_0^2 + q_1^2 - q_2^2 - q_3^3\right)/2 & q_1 q_2 - q_0 q_2 & q_1 q_3 + q_0 q_2 \\ q_1 q_2 + q_0 q_3 & \left(q_0^2 - q_1^2 + q_2^2 - q_3^3\right)/2 & q_2 q_3 - q_0 q_1 \\ q_1 q_3 - q_0 q_2 & q_2 q_3 + q_0 q_1 & \left(q_0^2 - q_1^2 - q_2^2 + q_3^3\right)/2 \end{bmatrix}. \tag{A5}$$

To completely determine the system in space, the time derivative of quaternion moments, $\dot{q}$, must be given. This reads as follows:

$$\begin{bmatrix} \dot{q}_0 \\ \dot{q}_1 \\ \dot{q}_2 \\ \dot{q}_3 \end{bmatrix} = \frac{1}{2}\omega q = \frac{1}{2}\begin{bmatrix} 0 & -\omega_1 & -\omega_2 & -\omega_3 \\ -\omega_1 & 0 & \omega_3 & \omega_2 \\ \omega_2 & \omega_3 & 0 & -\omega_1 \\ \omega_3 & -\omega_2 & -\omega_1 & 0 \end{bmatrix}\begin{bmatrix} q_0 \\ q_1 \\ q_2 \\ q_3 \end{bmatrix}, \tag{A6}$$

where index 1, 2, and 3 for ω refer to the x, y, and z Cartesian components of the angular velocity in the fixed space frame, respectively.

For the details see the references.[38,40]

[1] J. R. Errington and P. G. Debenedetti, "Relationship between structural order and the anomalies of liquid water," Nature (London) **409**, 318 (2001).
[2] R. J. Speedy and C. A. Angell, "Isothermal compressibility of supercooled water and evidence for a thermodynamic singularity at −45 °C," J. Chem. Phys. **65**, 851 (1976).
[3] H. L. Pi, J. L. Aragones, C. Vega, E. G. Noya, J. L. F. Abascal, M. A. Gonzalez, and C. McBride, "Anomalies in water as obtained from computer simulations of the tip4p/2005 model: Density maxima, and density, isothermal compressibility and heat capacity minima," Mol. Phys. **107**, 365 (2009).
[4] A. Luzar and D. Chandler, "Hydrogen-bond kinetics in liquid water," Nature (London) **379**, 55 (1996).
[5] R. Kumar, J. R. Schmidt, and J. L. Skinner, "Hydrogen bonding definitions and dynamics in liquid water," J. Chem. Phys. **126**, 204107 (2007).
[6] D. Paschek, A. Rüppert, and A. Geiger, "Thermodynamic and structural characterization of the transformation from a metastable low-density to a very high-density form of supercooled tip4p-ew model water," ChemPhysChem **9**, 2737 (2008).
[7] S. Garrett-Roe, F. Rao, and P. Hamm, "Structural inhomogeneity of water by complex network analysis," J. Phys. Chem. B **114**, 15598 (2010).
[8] P. Hamm, D. Prada-Gracia, R. Shevchuk, and F. Rao, "Towards a microscopic description of the free-energy landscape of water," J. Chem. Phys. **137**, 144504 (2012).
[9] C. Vega and J. L. F. Abascal, "Simulating water with rigid non-polarizable models: A general perspective," Phys. Chem. Chem. Phys. **13**, 19663 (2011).
[10] A. Pelizzola, C. Buzano, E. De Stefanis, and M. Pretti, "Two-dimensional lattice-fluid model with waterlike anomalies," Phys. Rev. E **69**, 061502 (2004).
[11] M. Karplus, "The Levinthal paradox: yesterday and today," Folding Des. **2**, S69 (1997).
[12] M. Cieplak and S. Niewieczerzal, "Hydrodynamic interactions in protein folding," J. Chem. Phys. **130**, 124906 (2009).
[13] F. Rao and A. Caflisch, "The protein folding network," J. Mol. Biol. **342**, 299 (2004).
[14] P. J. Feibelman, "The first wetting layer on a solid," Phys. Today **63**(2), 34 (2010).
[15] S. Succi, *The Lattice Boltzmann Equation* (Oxford, Science, 2001).
[16] D. Wolf-Gladrow, *Lattice-Gas Cellular Automata and Lattice Boltzmann Models* (Springer, 2000).
[17] S. Succi, R. Benzi, and M. Vergassola, "The lattice Boltzmann equation: Theory and applications," Phys. Rep. **222**, 145 (1992).
[18] S. Chen and G. Doolen, "Lattice Boltzmann method flow for fluid flows," Annu. Rev. Fluid Mech. **30**, 329 (1998).
[19] S. Succi, "Lattice Boltzmann across scales: from turbulence to DNA translocation," Eur. Phys. J. B **64**, 471 (2008).
[20] F. Farahpour, A. Maleknejad, F. Varnik, and M. R. Ejtehadi, "Chain deformation in translocation phenomena," Soft Matter **9**, 2750 (2013).
[21] M. Fyta, S. Melchionna, S. Succi, and E. Kaxiras, "Hydrodynamic correlations in the translocation of biopolymer through a nanopore: Theory and multiscale simulations," Phys. Rev. E **78**, 036704 (2008).
[22] C. K. Aidun and J. R. Clausen, "Lattice-Boltzmann method for complex flows," Annu. Rev. Fluid Mech. **42**, 439 (2010).
[23] N. Moradi, F. Varnik, and I. Steinbach, "Roughness-gradient induced spontaneous motion of droplets on hydrophobic surfaces: A lattice Boltzmann study," EPL **89**, 26006 (2010).
[24] N. Moradi, F. Varnik, and I. Steinbach, "Contact angle dependence of the velocity of sliding cylindrical drop on flat substrates," EPL **95**, 44003 (2011).
[25] S. Zaleski, J. Li, and S. Succi, "Two-dimensional Navier-Stokes simulation of deformation and breakup of liquid patches," Phys. Rev. Lett. **75**, 244 (1995).
[26] S. Succi, G. Amati, and R. Piva, "Massively Parallel Lattice-Boltzmann Simulation of Turbulent Channel Flow," Int. J. Mod. Phys. C **8**, 869 (1997).
[27] M. Mazzeo and P. V. Coveney, "HemeLB: A high performance parallel lattice-Boltzmann code for large scale fluid flow in complex geometries," Comput. Phys. Commun. **178**, 894 (2008).
[28] A. Ben-Naim, "Statistical mechanics of 'waterlike' particles in two dimensions. I. Physical model and application of the Percus-Yevick equation," J. Chem. Phys. **54**, 3682 (1971).
[29] I. Mazzitelli, M. Venturoli, S. Melchionna, and S. Succi, "Towards a mesoscopic model of water-like fluids with hydrodynamic interactions," J. Chem. Phys. **135**, 124902 (2011).
[30] A. Ben-Naim, *Water and Aqueous Solutions. Introduction to a Molecular Theory* (Plenum Press, New York, 1974).
[31] A. Ben-Naim, *Molecular Theory of Water and Aqueous Solutions: Part I: Understanding Water* (World Scientific Publishing Company, 2010).
[32] L. D. Landau, *Fluid Mechanics, Course of Theoretical Physics*, Vol. 6 (Pergamon Press Ltd., Oxford, England, 1987).
[33] E. P. Gross, P. L. Bhatnagar, and M. Krook, "A model for collision processes in gases. I. Small amplitude processes in charged and neutral one-component systems," Phys. Rev. **94**, 511 (1954).
[34] Y. H. Qian *et al.*, "Lattice BGK models for Navier-Stokes equation," EPL **17**, 479 (1992).
[35] A. D. J. Haymet, K. A. T. Silverstein, and K. A. Dill, "A simple model of water and the hydrophobic effect," J. Am. Chem. Soc. **120**, 3166 (1998).
[36] C. Dias *et al.*, "Microscopic Mechanism for Cold Denaturation," Phys. Rev. Lett. **100**, 118101 (2008).
[37] T. Hynninen *et al.*, "A molecular dynamics implementation of the 3D Mercedes-Benz water model," Comput. Phys. Commun. **183**, 363 (2012).
[38] D. C. Rapaport, "Molecular dynamics simulation using quaternions," Biophys. Chem. **60**, 306 (1985).
[39] J. Horbach and S. Succi, "Lattice Boltzmann versus molecular dynamics simulation of nano-hydrodynamic flows," Phys. Rev. Lett. **96**, 224503 (2006).
[40] E. A. Coutsias and L. Romero, "The quaternions with an application to rigid body dynamics," Sandia National Laboratories, Technical Report SAND2004-0153 (2004).